TENSILE PROPERTIES OF DEEP DRAWN IN-SITU POLYMERIZED FIBER-METAL-LAMINATES

Conference Paper · June 2022

CITATIONS
0

READS
5

3 authors, including:

Henrik Werner
Karlsruhe Institute of Technology
11 PUBLICATIONS **81** CITATIONS

SEE PROFILE

TENSILE PROPERTIES OF DEEP DRAWN IN-SITU POLYMERIZED FIBER-METAL-LAMINATES

Henrik Oliver Werner[a,b], Wilfried Liebig [a], Kay André Weidenmann [c]

a: Karlsruhe Institute of Technology (KIT), Institute for Applied Materials, Karlsruhe, Germany – henrik.werner@kit.edu
b: Karlsruhe Institute of Technology (KIT), Institute of Vehicle System Technology, Karlsruhe, Germany
c: University of Augsburg, Institute of Materials Resource Management – Hybrid Composite Materials (MRM), Augsburg, Germany

Abstract: *In previous work, we have introduced a new manufacturing process, which combines deep drawing with thermoplastic resin transfer molding. The fabric is infiltrated with a reactive resin during forming, which polymerizes to a tough poly (methyl methacrylate) matrix after completion of the forming process. In this contribution, miniaturized tensile specimen are tested. The tensile properties are location dependent due to the forming process. It is found, that FMLs Young's modulus and yield strength depends on the Young's modulus and yield strength of the metal. The ultimate tensile strength of the FML depends on the GFRP layer and its fiber orientation, as well as fiber volume content. Specimens with a ± 45° fiber orientation show higher failure strains compared to specimens with 0° and 90° fiber orientation.*

Keywords: FML; multi-material design; deep-drawing; sandwich; in-situ polymerization

1. Introduction

The climate change is the greatest challenge of our time. Sustainability has thus become a central issue in society, as well as in the design process of new products. Lightweight design is no longer considered exclusively under technical, but also under ecological boundary conditions. One example is the automotive industry, which has to reduce the CO_2 emissions of its vehicle fleet through legal framework conditions [1]. The automobile's energy consumption occurs 87 % of live time cycle during use and is thus proportional to the vehicle mass [2]. The result is the electrification of the powertrain and the use of new lightweight materials and strategies. In addition to steel and aluminum sheets [3], fiber-reinforced composites (FRP) are increasingly being used in car body design [4]. Joining or combining materials of different material classes has therefore become an essential part of the development process. Fiber-metal-laminates (FML) are a special form of multi-material design and combine the advantageous properties of metals and FRPs in a single layered material. FMLs exhibit excellent resistance to crack propagation, impact, and flammability [5].

In the 1980s, FMLs were developed and commercialized for the civil aviation industry [6,7]. The classical autoclave manufacturing process is time consuming, expensive, and the achievable geometric complexity of the components is low [8,9]. For mass production of FML components, the material and process costs have to be reduced and the producible complexity of the components has to be increased. A possible process could be the combination of deep drawing and thermoplastic resin transfer molding (T-RTM), as shown in Figure 1. In this one-step process,

  doi:10.5075/epfl-298799_978-2-9701614-0-0

an in-situ polymerizing matrix is injected during deep drawing. The metal sheets and the fabric layers are formed simultaneously, while the matrix infiltrates the fabrics. The matrix polymerizes after the deep drawing process, embedding the fibers and bonding the FRP to the metal sheets [10–16], shown in Figure 1. The mechanical properties of the FML are strongly influenced by the manufacturing process of the generic part geometry. Therefore, the mechanical properties have to be determined dependent on the generic part geometry, otherwise the structure-property relationships cannot be measured. For this purpose, tensile specimens from four regions of the generic part are extracted, shown in Figure 1. The regions differ in terms of their forming history, more precisely the degree of metal forming, fiber draping and infiltration.

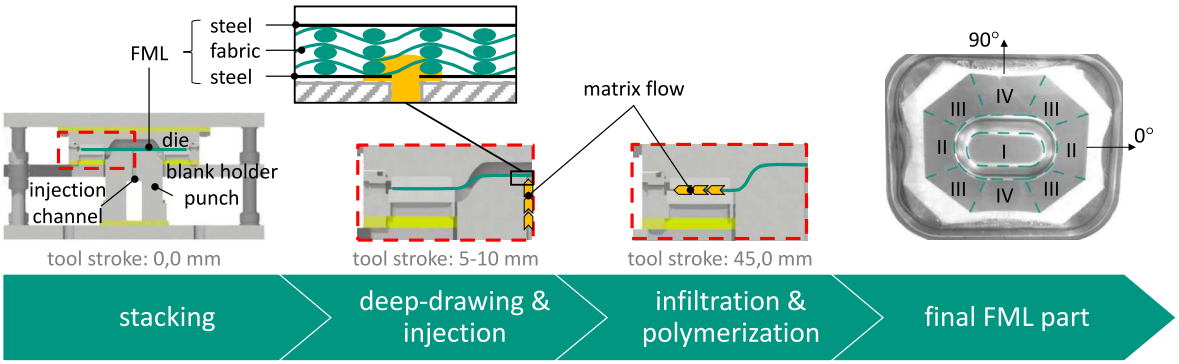

Figure 1. Process flow of combined deep drawing and resin transfer molding

2. Material

The FML layup is a sandwich construction with metal sheets as face sheets and thermoplastic reinforced twill weave fabrics as intermediate layer. The DC04 metal sheet thickness is 1 mm and six plies of 280 g/m² E-glass twill weave fabric 2/2 (Interglas 92125 FK800) are used. As resin system, a 1:1 mixture of acrylates Elium 130 and Elium 190 from Arkema S.A. with 2.5 % dibenzoyl peroxide (United Initiators, BP-50-FT) is used. The rolling direction of the metal sheet defines the 0° orientation, which is equal to the weft direction of the dry fabrics. In weft direction (0°), the fabric weight is 143 g/m² and 133 g/m² in warp direction (90°). The metal sheets were pretreated to increase the adhesion to the thermoplastic matrix according to [17] with manual grinding and a silane adhesion promoter (Evonik, Glymo). In addition, generic parts are produced with aluminum sheets of 1 mm AA5182-H111 and six plies of 280 g/m² E-glass twill weave fabric. The aluminum sheets are pretreated with release agent to be able to remove them after the manufacturing process to obtain GFRP parts without metal sheets. The draping influence of the fibers on the tensile properties of the FML is investigated using the GFRP parts.

The generic part geometry is divided into four general regions with different forming histories according to Figure 1. The samples are extracted by waterjet cutting from four different FML parts and two GFRP parts with equivalent process settings. The average fiber volume content of all parts is 70 % ± 3 % and is measured by thermal gravimetric analysis by the Fraunhofer Institute for Chemical Technology.

3. Experimental set-up

The tensile tests are performed on a Zwick/Roell ZMART.PRO 200 kN universal testing machine. The specimens are chosen according to DIN EN ISO 527-4:2022-03 [18] and ASTM D3039/D3039M−17 [19] with dimensions of 60 mm x 10 mm x 3 mm (LxBxt). For clamping 20

  doi:10.5075/epfl-298799_978-2-9701614-0-0

mm are required on each side, resulting in a free measuring length of 20 mm. Wooden spacers with a are placed between the clamping jaws due to the short clamping length. This prevents the clamping jaws from tilting. Strain is measured by using two-dimensional digital image correlation (GOM GmbH, Aramis 4M) with a recording frequency of 2 Hz for the FML specimens and 5 Hz for the GFRP specimens. An airbrush pistol with body paint is used for the speckled stochastic pattern to obtain a fine pattern for high resolution for high strains. The FML specimens are clamped rotated by 90° to measure the strain in stacking direction ε_z, shown in Figure 2. The GFRP specimens are not rotated and the transverse strain ε_y is recorded. The transverse velocity is v = 2 mm/min and corresponds to a strain rate of $\dot{\varepsilon}$ = 0.0016 1/s. A prestress of 2 MPa is applied via hydraulic jaws with a hydraulic pressure of 20 bar. Stresses and strains are calculated homogenized over the entire cross-section of the specimens. The Young's modulus is determined for strains between ε_x = 0.01 % and 0.07 % according to ASTM E1111 [20] by using linear regression with the method of least squares. The 0.05 % yield strength is determined as $R_{p0.05}$ for a plastic strain of ε_x = 0.05 %. The tensile strength R_m is calculated from the maximum measured force F.

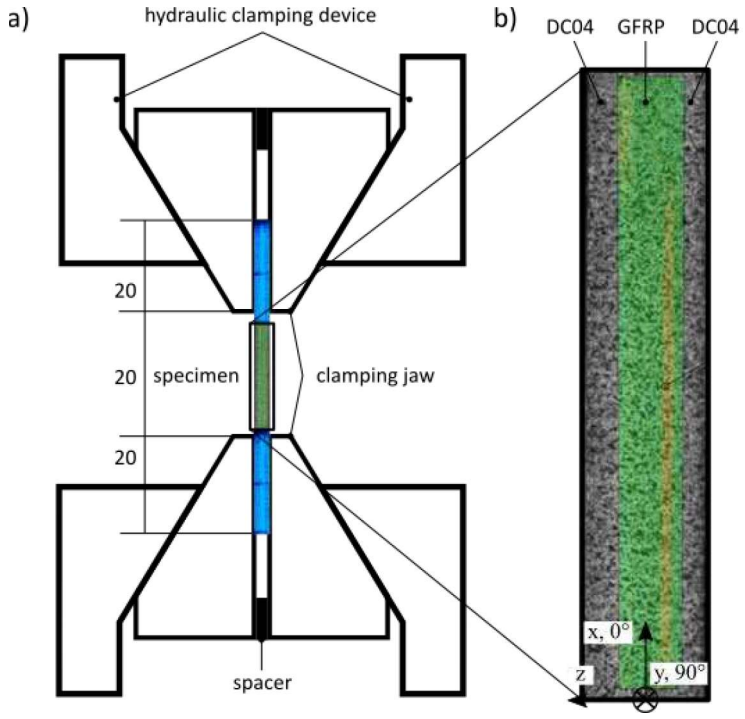

Figure 2. a) Experimental set up for tensile test with b) measured strain field of 2D-DIC system on a FML specimen

4. Results

Figure 3 summarizes the results in the form of box-plots. The tensile properties $(E, R_{p0.05}, R_m, e_b)$ show a strong dependence on region and orientation for the FML, as well as for the GFRP specimens. In general, the 0° orientation exhibits higher tensile properties than the 90° orientation within the respective region, with the exception of the FML specimens from region IV. The qualitative difference between 0° and 90° orientation is noticeable for all mentioned properties and is especially pronounced for ultimate tensile strength, except for FML specimen from region IV. The 45° orientation shows higher Young's modulus, yield strength and ultimate tensile strength compared to the 135° orientation for FML and GFRP specimens. The

  doi:10.5075/epfl-298799_978-2-9701614-0-0

highest failure strain is reached by the 135° orientation with $e_b \approx 6$ % for GFRP and $e_b \approx 10$ % for FML specimens compared to $e_b \approx 2$ % for FML and GFRP specimens in 0° and 90° orientation.

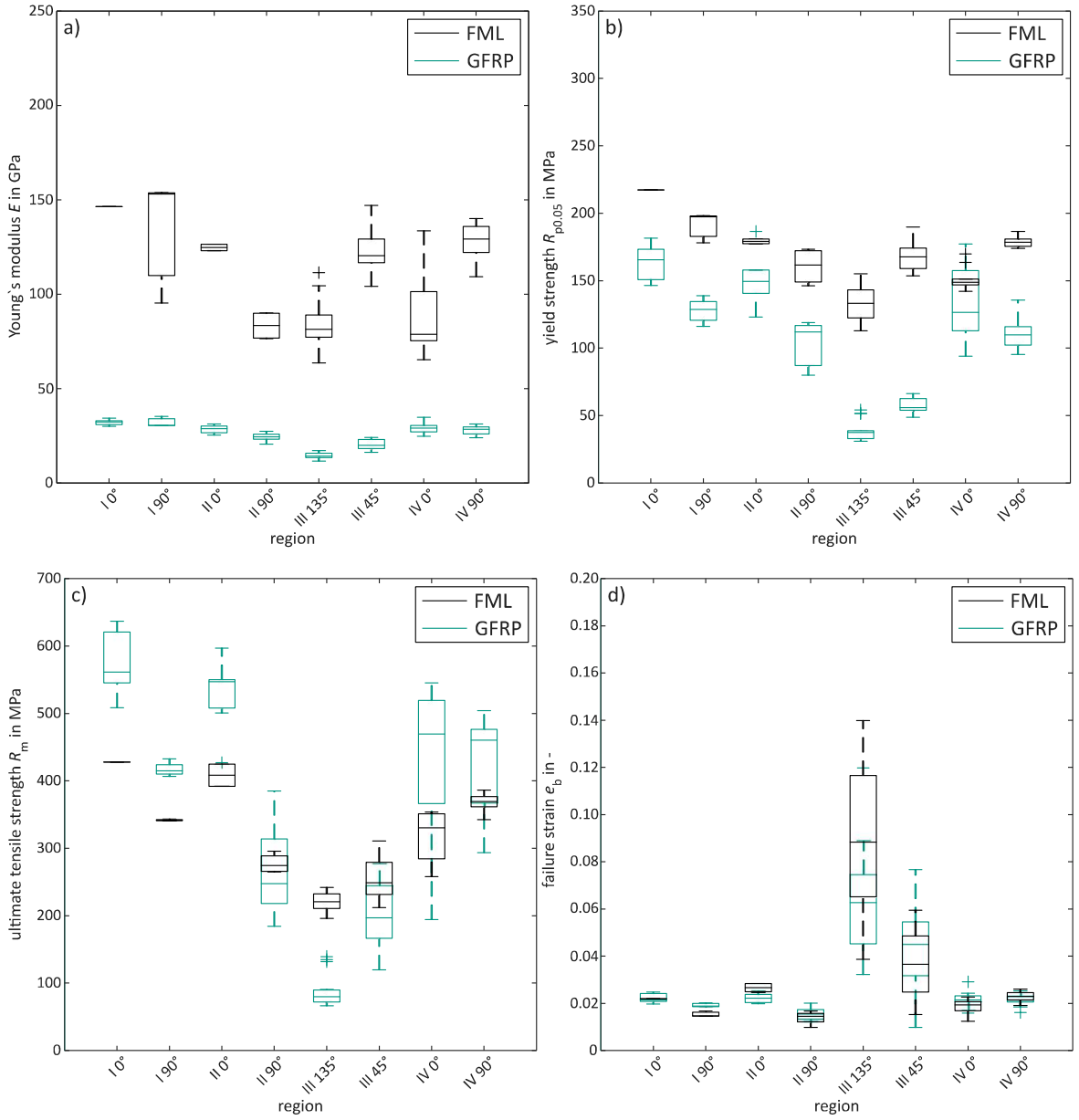

Figure 3. Box-plots of region dependent mechanical properties of GFRP and FML specimens a) Young's modulus, b) yield strength, c) ultimate tensile strength and d) failure strain

The stress-strain curves of the GFRP specimens in Figure 4 are linear elastic in 0° and 90° orientation, while in 45° and 135° orientation they are strongly nonlinear. The GFRP specimens in Figure 4 c) oriented in 135° show nearly ideal plastic flow behavior and differs from the stress-strain curve of 45° oriented specimens. All stress-strain curves of the FML specimens in 0° and 90° orientation show a bi-linear behavior, with a pronounced yield point. In 45° and 135° orientation, the stress-strain curves are strongly nonlinear and qualitatively similar to those from the GFRP specimens. In Figure 4 b) for region II, the stress-strain curves of GFRP and FML specimens oriented in 90° show significantly lower ultimate tensile strength. The ultimate tensile strength of GFRP and FML correlates directly. The same observation applies to the stress-strain behavior for GFRP and FML specimens in Figure 4 c) with 45° and 135° orientation and

  doi:10.5075/epfl-298799_978-2-9701614-0-0

less pronounced in Figure 4 a) with 0° and 90° orientation. As already mentioned for the box-plots, region IV in Figure 4 d) is an exception and shows no correlation between stress-strain behavior of GFRP and FML.

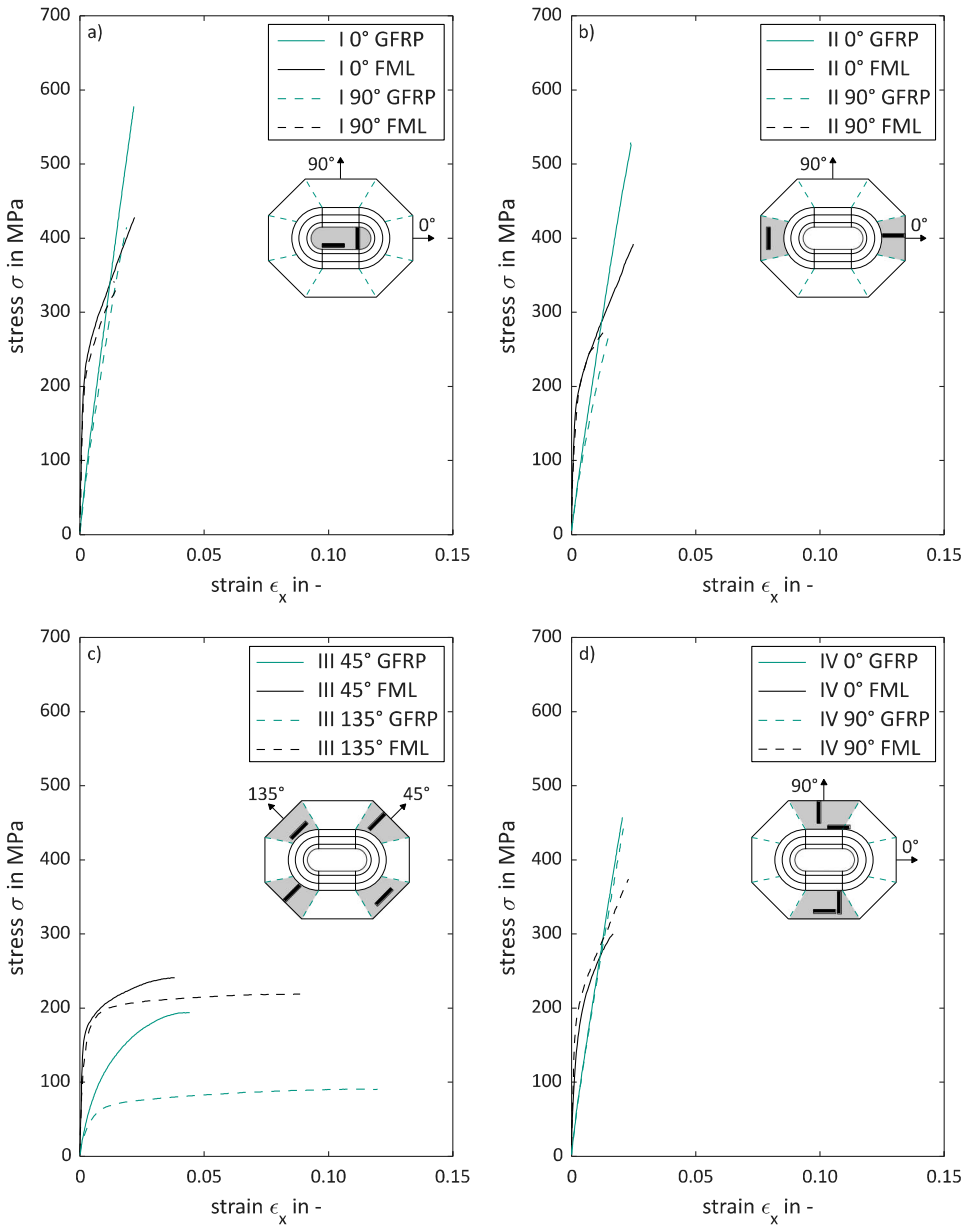

Figure 4. Representative stress-strain curves of GFRP and FML specimens from a) region I in 0° and 90° orientation, b) region II in 0° and 90° orientation, c) region III in 45° and 135° orientation and d) region IV in 0° and 90° orientation

5. Discussion

In region II and in region IV the fibers are drawn-in towards the center of the generic part. The fibers in 90° orientation in region II are draped transverse to loading direction. This results in a high fiber curvature and thus in low tensile properties. The same applies for the specimens in region IV in 0° orientation. Due to the shorter length of the geometry in region II compared to region IV, the fibers curvature is higher in region II, as shown in Figure 5.

  doi:10.5075/epfl-298799_978-2-9701614-0-0

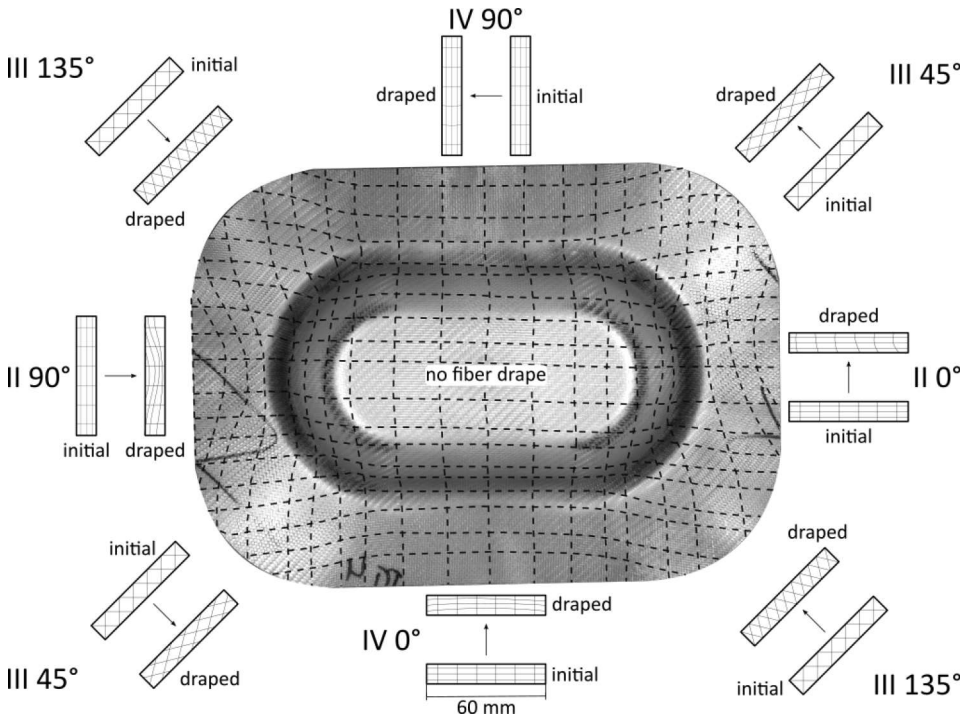

Figure 5. Fiber draping of representative generic GFRP part with removed metal sheets

The observed results can be explained by an analogous model consisting of two parallel springs representing the two metal layers and the GFRP layer [13]. The load distribution between the two layers, respectively the two springs, depends on the spring stiffness

$$c = \frac{EA}{L} \rightarrow \frac{c_1}{c_2} = \frac{E_1 t_1}{E_2 t_2} \tag{1}$$

with the Young's modulus E, the cross-section $A = bt$ and the length L, width b of the specimen and thickness t of the respective layer. The pronounced yield point of the FML stress-strain curves in Figure 4 is the load transition point between metal layers and GFRP layer. The stiffer DC04 metal sheets carry the main load up to the yield strength and then transfer the load to the GFRP layer. The GFRP layers ultimate tensile strength determines the ultimate tensile strength of the FML specimen, which depends on the fiber orientation of the GFRP layer due to fiber draping during forming. The more fibers are oriented in tensile direction, the higher is the ultimate tensile strength. The yield strength of the FML specimens depends on the degree of metal forming. For example, the influence of the GFRP yield strength on the FML yield strength is not be seen in Figure 3 b) for region I with 90° orientation and region III with 45° orientation, while the influence of the GFRP ultimate tensile strength correlates directly with the FMLs ultimate tensile strength in Figure 3 c) and failure strain in Figure 3 d). In region III with 45° orientation, the fibers are draped in loading direction, while in 135° orientation, the fibers are draped in transverse direction and the specimens have the largest proportion of fibers in transverse direction, which is why they have the lowest mechanical properties. The orientation and curvature of the fibers to the direction of loading significantly affects the ultimate tensile strength, as can be seen in Figure 4 b) and c). The specimens with higher fiber curvature in Figure 5, region II 90° and region III 135°, have lower tensile properties. This can also be seen in Figure 4 d) for the region IV with 0° and 90° orientation, with the 0° specimens exhibiting higher fiber curvatures due to draping and thus show lower tensile properties compared to the 90° orientation.

  doi:10.5075/epfl-298799_978-2-9701614-0-0

6. Conclusion

Results of tensile tests on GFRP and FML specimens of generic parts manufactured by combined deep-drawing with in-situ polymerization are presented. The study demonstrated that the mechanical properties in terms of Young's modulus, yield strength, ultimate tensile strength and failure strain are location dependent due to the forming process. The tested GFRP specimens show the influence of fiber draping due to forming on the tensile properties. The FMLs ultimate tensile strength and failure strain are dominated by the GFRP, while the results show no influence of the GFRPs Young's modulus and yield strength on the respective properties of the FML.

Acknowledgements

The German Research Foundation (DFG) kindly supports this research project (WE 4273/13-1 & -2, HE 6154/4-1 & -2). The Fraunhofer Institute for Chemical Technology kindly supports the manufacturing of the laminates. ARKEMA SA Colombes (France) kindly provided the polymer. United Initiators provided the peroxide and Evonik the coupling agent. The authors also thank their colleges for support, especially Thomas Mennecart from the IUL of the TU Dortmund and Moritz Kruse from the PPI of the Leuphana University Lüneburg for the great collaboration.

7. References

[1] European Parliament. Regulation (EU) 2019/631 of the European Parliament and of the Council of 17 April 2019 setting CO2 emission performance standards for new passenger cars and for new light commercial vehicles, and repealing Regulations (EC) No 443/2009 and (EU) No 510/2011; 2021.

[2] Mayyas A, Qattawi A, Omar M, Shan D. Design for sustainability in automotive industry: A comprehensive review. Renewable and Sustainable Energy Reviews 2012;16(4):1845–62. https://doi.org/10.1016/j.rser.2012.01.012.

[3] Tisza M, Czinege I. Comparative study of the application of steels and aluminium in lightweight production of automotive parts. International Journal of Lightweight Materials and Manufacture 2018;1(4):229–38. https://doi.org/10.1016/j.ijlmm.2018.09.001.

[4] Dröder K, Vietor T (eds.). Technologies for economical and functional lightweight design. Berlin, Heidelberg: Springer Berlin Heidelberg; 2019.

[5] Vlot A, Vogelesang LB, Vries TJ de. Towards application of fibre metal laminates in large aircraft. Aircraft Eng & Aerospace Tech 1999;71(6):558–70. https://doi.org/10.1108/00022669910303711.

[6] Vogelesang L, Vlot A. Development of fibre metal laminates for advanced aerospace structures. Journal of Materials Processing Technology 2000;103(1):1–5. https://doi.org/10.1016/S0924-0136(00)00411-8.

[7] Vlot A. Glare: History of the development of a new aircraft material. Dordrecht: Kluwer Acad. Publ; 2001.

[8] Gunnink JW, Vlot A, Vries TJ de, van der Hoeven W. Glare Technology Development 1997–2000. Appl Compos Mater 2002;9(4):201–19. https://doi.org/10.1023/A:1016006314630.

[9] Sinke J. Manufacturing of GLARE Parts and Structures. Appl Compos Mater 2003;10(4/5):293–305. https://doi.org/10.1023/A:1025589230710.
[10] Mennecart T, Werner H, Ben Khalifa N, Weidenmann KA. Developments and Analyses of Alternative Processes for the Manufacturing of Fiber Metal Laminates. In: Volume 2: Materials; Joint MSEC-NAMRC-Manufacturing USA. American Society of Mechanical Engineers; 2018.
[11] Werner HO, Dörr D, Henning F, Kärger L. Numerical modeling of a hybrid forming process for three-dimensionally curved fiber-metal laminates. In: Proceedings of the 22nd International ESAFORM Conference on Material Forming: ESAFORM 2019. AIP Publishing; 2019, p. 20019.
[12] Werner HO, Stern C, Weidenmann KA. Location-Dependent Mechanical Properties of In-Situ Polymerized Three-Dimensional Fiber-Metal Laminates. In: Hausmann JM, editor. 22nd Symposium on Composites. Zurich: Trans Tech Publications Limited; 2019.
[13] Werner HO, Liebig W, Weidenmann KA. Mechanical Properties of In-Situ Polymerized Fiber-Metal-Laminates. In: Hausmann JM, Siebert M, Hehl A von, Weidenmann KA, editors. Proceedings 4th International Conference Hybrid 2020 Materials and Structures; 2020.
[14] Werner HO, Poppe C, Henning F, Kärger L. Material Modeling in Forming Simulation of Three-Dimensional Fiber-Metal-Laminates – A Parametric Study. In: 23rd International Conference on Material Forming (ESAFORM 2020); 2020, p. 154–161.
[15] Werner HO, Schäfer F, Henning F, Kärger L. Material Modelling of Fabric Deformation in Forming Simulation of Fiber-Metal Laminates – A Review on Modelling Fabric Coupling Mechanisms. In: 24th International Conference on Material Forming; 2021.
[16] Mennecart T, Gies S, Ben Khalifa N, Tekkaya AE. Analysis of the Influence of Fibers on the Formability of Metal Blanks in Manufacturing Processes for Fiber Metal Laminates. JMMP 2019;3(1):2. https://doi.org/10.3390/jmmp3010002.
[17] Werner H, Sönmez I, Wendel R, Henning F, Weidenmann KA. Characterization of the interlaminar shear strength of fiber metal laminates with reactive processed thermoplastic matrix. In: SAMPE Europe Conference & Exhibition 2017 Stuttgart: Stuttgart, Germany, 14-16 November 2017. Red Hook, NY: Curran Associates Inc; 2017.
[18] Deutsches Institut für Normung e. V. DIN EN ISO 527-4:2022-03, Kunststoffe - Bestimmung der Zugeigenschaften - Teil 4: Prüfbedingungen für isotrop und anisotrop faserverstärkte Kunststoffverbundwerkstoffe (ISO 527-4:2021); Deutsche Fassung EN ISO 527-4:2021. Berlin: Beuth Verlag GmbH; 2022. https://doi.org/10.31030/3328116.
[19] D30 Committee. Test Method for Tensile Properties of Polymer Matrix Composite Materials. West Conshohocken, PA: ASTM International. https://doi.org/10.1520/D3039_D3039M-17.
[20] E28 Committee. Test Method for Youngs Modulus, Tangent Modulus, and Chord Modulus. West Conshohocken, PA: ASTM International. https://doi.org/10.1520/E0111-04R10.

